Supplementary Information

Plasmonic-enhanced Targeted Nanohealing of Metallic Nanostructures

Hangbo Yang[†], Jinsheng Lu[†], Pintu Ghosh[†], Ziyao Chen[†], Wei Wang[†], Hui Ye[†], Qian Yu[‡], Min Qiu[*, †], and Qiang Li[*, †]

[†]State Key Laboratory of Modern Optical Instrumentation, College of Optical Science and Engineering, Zhejiang University, Hangzhou, 310027, China

[‡]Center of Electron Microscopy and State Key Laboratory of Silicon Materials, Department of Materials Science & Engineering, Zhejiang University, Hangzhou, 310027, China

E-mail: qiangli@zju.edu.cn

1. Experimental apparatus

Figure S1 shows the experimental apparatus for nanohealing and electrical characterization. A continuous-wave (CW) laser (λ = 532 nm) beam sequentially passes through the first polarizer (Glan-Taylor laser polarizer), a mirror, the second polarizer, a half-wave plate, a mechanical shutter, and a Pellicle beam splitter. Finally, the laser beam is focused on the nanogap by an objective (100×, Mitutoyo Microscope). The mechanical shutter, the half-wave plate and the combination of the two polarizers control the exposure time, the polarization, and the exposure power on the nanogaps, respectively. For precise positioning of the laser focus, a three-axis translation stage with piezoelectric control (30 nm in accuracy) is utilized. A two-probe (micro-tungsten probe) system is used as an electrical characterization module to measure the V-I curve of the whole nanostructure. The resistance is obtained from the measured V-I curve.

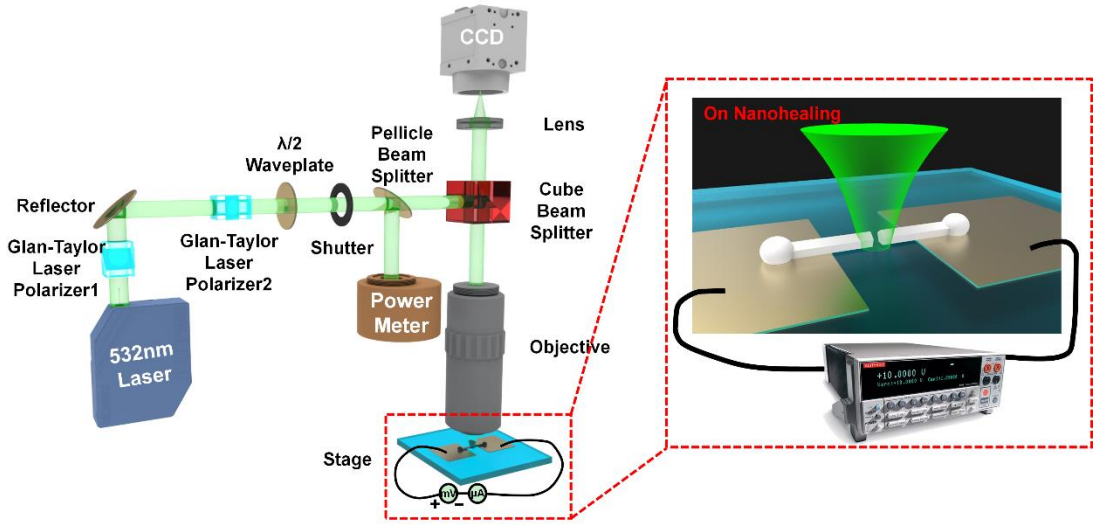

Figure S1. Schematic diagram of the experimental apparatus for nanohealing and electrical characterization

2. Simulation results corresponding to nanohealing.

To unveil the physical mechanisms behind the nanohealing, electromagnetic field, heat power density, and temperature distributions of nanogaps are calculated with the commercial software packages FDTD and COMSOL Multiphysics (see Methods). In the simulations (Figure S2), a nanogap (g = 80 nm) between two NWs (D = 300 nm) is on a silica substrate. The Gaussian light beam (λ = 532 nm, P = 30 mW, and R_b = 200 nm) with perpendicular polarization (in y direction), which is incident from top (*i.e.* negative Z-direction), is focused on the nanogap. For simplicity, we only consider the steady-state case for the temperature calculation as the exposure time (2 ms) of the laser shots is much longer than thermal response time (of the order of nanoseconds).[1] The heat power density is related to the electric field E by $Q = 0.5\varepsilon_0\omega\mathrm{Im}(\varepsilon_r)|E|^2$,[2] where Q is the heat power density ; ε_0 and ε_r (= -11.76 + 0.37i) are vacuum permittivity and relative permittivity of silver, respectively; ω is the frequency of the incident laser light. The spatial distribution of the temperature (T) is obtained by solving the steady-state heat transfer equation $k\nabla^2 T + Q = 0$, where k is the thermal conductivity (170 W/(m·K) for silver NW, the size effect of which is taken into account).[1,3-5]

The excited electric fields predominantly concentrate in the four lower corners in the nanogap (Figure S2(a, b)).[6-8] Heat is produced only in the silver because of its imaginary part of the permittivity. Consequently, the heat power mainly concentrates in the four lower corners (Figure S2(c, d)) of NW surfaces facing the nanogap, and high temperature can be found in the nanogap and its surroundings (Figure S2(e)). Due to the high thermal conductivity of silver and small cross-section of the silver NWs, temperature distribution in the cross-section of the silver NW close to the nanogap is almost uniform (Figure S2(f)). As a result, the local silver atoms gradually move to the

nanogap. Once the laser exposure is terminated, the local temperature in the nanogap decreases. During this decline of local temperature, the resolidification of local movable silver atoms narrows the gap and partial connection of NWs is achieved.

Figure S2(g) shows the simulated maximum temperature of the nanogaps with different widths versus the NW diameters at P = 40 mW (the power used in experiments for g = 80 nm, 40 nm, and 20 nm). The simulated maximum temperature of the nanogaps at P=30 mW (the initial power used in experiments) for nanogaps with width g = 80 nm is also included. It can be observed that the maximum temperatures of the nanogaps decrease as the diameters of the NWs increase from 220 nm to 340 nm. Therefore, higher power is required to maintain the same temperature rise at larger diameters (to be shown in Figure 2(d) in the manuscript). The maximum temperatures of the nanogaps also decrease as the nanogap widths decrease from 80 nm to 20 nm at P = 40 mW.

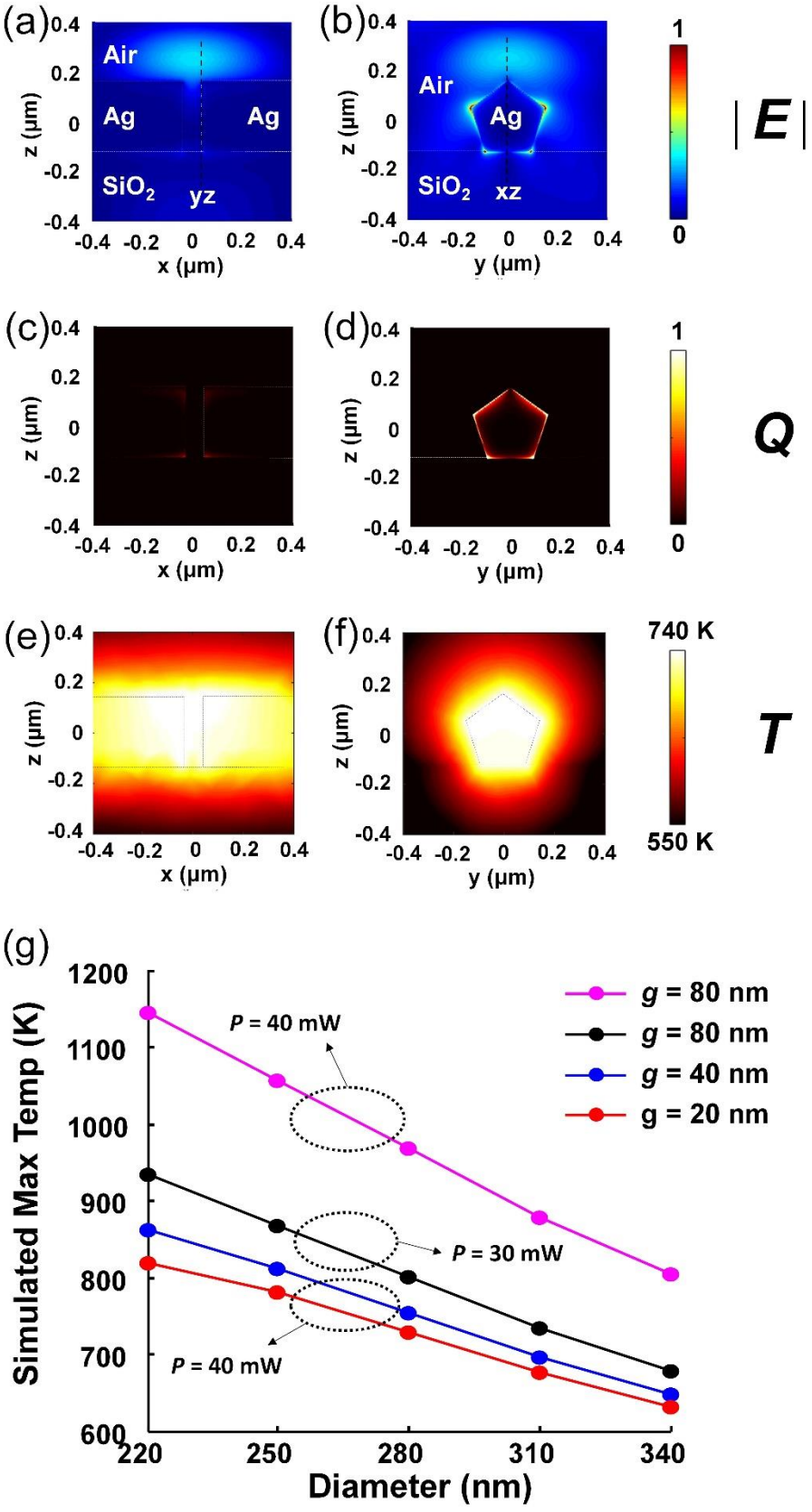

Figure S2. Simulation results corresponding to nanohealing. Simulated (a, b) electric

field, (c, d) heat power density, and (e, f) temperature distributions for a nanogap (g = 80 nm) between two NWs (D = 300 nm) for incident laser beam with perpendicular polarization (*i.e.* in y direction). (a, c, and e) Simulated results for the longitudinal section (bisecting the NWs along the longest axis) marked by the black dash line in (b). (b, d, and f) Simulated results for the pentagonal cross-section of the nanogap marked by the black dash line in (a). (g) Simulated maximum temperature versus NW diameters for four nanogaps. One nanogap with width g = 80 nm (black dots) is exposed to the laser with power P = 30 mW. Three nanogaps with widths g = 20 nm, 40 nm, and 80 nm (red, blue, and pink dots, respectively) are exposed to the laser with power P = 40 mW.

3. Simulations for polarization analysis

Figure S3 shows that the simulated maximum temperature of the nanogap is less sensitive to nanogap width under perpendicular polarization compared with that under parallel polarization of the incident laser beam. With the nanogap width increasing from 0 nm to 80 nm, the maximum temperature of the nanogap increases by 50 °C under perpendicular polarization (the black line), whereas it increases by 450 °C under parallel polarization (the blue line). The reason for this behavior is that the gap-mode is excited only for parallel polarization of the incident light beam, and the local electric field intensity at the nanogap is greatly enhanced by this gap-mode. However, the electric field intensity of gap-mode decreases gradually with nanogap width. Therefore, the local electric field intensity and the corresponding energy, which is converted to heat, also decreases, which, in turn, decreases the maximum temperature.

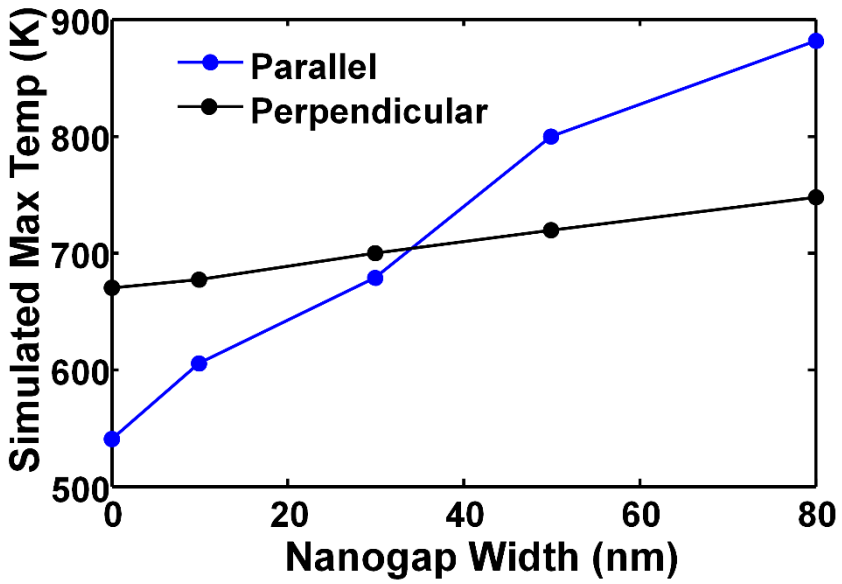

Figure S3. Simulated maximum temperature versus nanogap width under parallel and perpendicular polarization of the incident laser beam.

4. Simulation of the dependence of absorptance on wavelength

The relationship between the absorptance of Ag NW (D = 300 nm for the nanowire and g = 80 nm for the nanogap) and the laser wavelength is calculated (shown in Fig. S4). The absorptance is defined as the ratio of the absorbed power by the NW to the incident laser power. The absorptance decreases with the increasing laser wavelength from 400 to 1000 nm. Since the absorptance has a positive correlation with the maximum temperature of the nanogap, a short-wavelength laser is preferred for high energy efficiency. Therefore, we choose 532 nm laser with low cost and easy operation in the experiments.

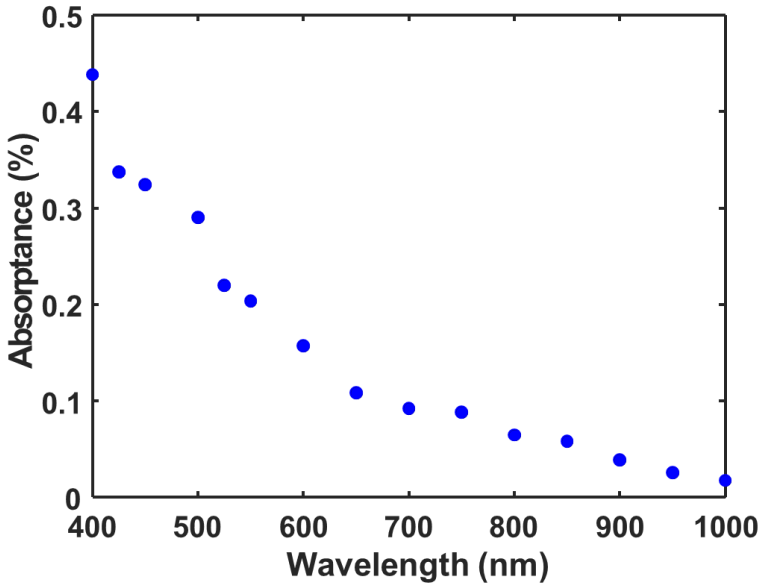

Figure S4 Simulated absorptance versus wavelength (D = 300 nm for the nanowire and g = 80 nm for the nanogap). The incident laser power is 30 mW.

5. Methods

Fabrication of the nanogaps in silver NWs. First, gold electrodes are fabricated by FIB on a 30-nm-thick gold film deposited on the silica substrate. The size of each electrode is about 150 μm × 250 μm which is large enough for electrical characterization. The width between two adjacent electrodes is about 10 μm. Second, silver NWs (synthesized by a self-seeding approach[9]) are laid between two adjacent electrodes by two nano-fiber probes. The NW diameters range from 200 nm to 400 nm, and the NWs are longer than 40 μm. In order to ensure good ohmic contacts between silver NWs and electrodes, NWs are welded on the electrodes by laser shots. The welded parts are depicted as hemispheres at the ends of NWs in Figure 1(a) in the manuscript. Third, nanogaps (g = 80 nm) in the middle of the NWs are fabricated by FIB.

Resistance Measurement. The apparatus for resistance measurement includes a source-

meter (Keithley 2602) and two tungsten micro-tapers. At first, two tungsten micro-tapers touch the electrodes connected with the NW with a nanogap. After the source-meter scans the voltage and its corresponding current, the V-I curve is obtained and the resistance of the whole structure (including a NW and two gold electrodes) is measured. If the resistance is above the range of the source-meter (10 MΩ), the nanogap is regarded as not healed. If the resistance is dozens of ohms (of the same order as of the whole NW before cutting), the nanogap is regarded healed. Therefore, the resistance measurement provides a criterion to check the healing of the nanogap.

Electromagnetic field simulation. Three-dimensional (3D) finite-difference time-domain (FDTD) method (FDTD Solutions v8.13, Lumerical) is used to obtain the electromagnetic field distribution with perfectly matched layers as absorbing boundary conditions. The mesh sizes across the NW cross-section and along the NW axis are taken as 2 nm and 5 nm, respectively. A Gaussian light source (λ = 532 nm) is focused on the nanogap (in the middle of the NW).

Thermal field simulation. From the FDTD results, the electric field distribution in the silver NW (including the nanogap) can be extracted and the heat power volume density Q can be calculated as $Q = 0.5\varepsilon_0\omega\mathrm{Im}(\varepsilon_r)|E|^2$.[10] This Q value is used as the heat source in COMSOL Multiphysics for simulating the temperature distribution. The thermal conductivities of silica and air are taken from the COMSOL library, and thermal conductivity of the silver NW is set as 170 W/(m·K), taking the size effect into consideration.[11] A fixed temperature of 293.15 K is set at the boundaries.

Reference

[1] L. Zhou, J. Lu, H. Yang, S. Luo, W. Wang, J. Lv, M. Qiu, and Q. Li, Appl. Phys. Lett. **110**, 081101 (2017).

[2] X. Chen, Y. Chen, M. Yan, and M. Qiu, ACS Nano **6**, 2550 (2012).

[3] Z. Cheng, L. Liu, S. Xu, M. Lu, and X. Wang, Sci. Rep. **5**, 10718 (2015).

[4] S. Dai, Q. Li, G. Liu, H. Yang, Y. Yang, D. Zhao, W. Wang, and M. Qiu, Appl. Phys. Lett. **108**, 121103 (2016).

[5] Q. Li, G. Liu, H. Yang, W. Wang, S. Luo, S. Dai, and M. Qiu, Appl. Phys. Lett. **108**, 193101 (2016).

[6] H. Wei, S. Zhang, X. Tian, and H. Xu, P. Natl.Acad. Sci. USA **110**, 4494 (2013)

[7] H. Yang, M. Qiu, and Q. Li, Laser Photonics Rev. **10**, 278 (2015).

[8] Z. Jia, H. Wei, D. Pan, and H. Xu, Nanoscale **8**, 20118 (2016).

[9] Y. Sun and Y. Xia, Adv. Mater. **14**, 833 (2002).

[10] X. Chen, Y. Chen, M. Yan, and M. Qiu, ACS Nano **6**, 2550 (2012).

[11] Z. Cheng, L. Liu, S. Xu, M. Lu, and X. Wang, Sci. Rep. **5**, 10718 (2015).